Journal of Inflammation Research

Dovepress
Taylor & Francis Group

Open Access Full Text Article

ORIGINAL RESEARCH

Gut Microbiota and Tryptophan Metabolism as Therapeutic Targets for Spinal Cord Injury: Insights From Probiotic Treatment

Jinwang Dong[1,2,*], Chen Xu[1,*], Shanshan Jin[3,*], Tao Xie[1,*], Zhengwei Xu[1], Dingjun Hao[1], Liang Dong[1]

[1]Department of Spine Surgery, Honghui Hospital, Xi'an Jiaotong University, Xi'an, Shaanxi, People's Republic of China; [2]School of Medicine, Yan'an University, Yan'an, Shaanxi, People's Republic of China; [3]Department of Rehabilitation, The second People's Hospital of Cao County of Shandong Province, Heze, Shandong, People's Republic of China

*These authors contributed equally to this work

Correspondence: Liang Dong, Email dongliang-526@163.com

Background: Probiotics have been demonstrated to repair spinal cord injuries (SCI) by improving gut microbiota dysbiosis; however, the specific mechanisms underlying their therapeutic effects on SCI remain incompletely elucidated.

Objective: This study aims to investigate the therapeutic effects of probiotics and analyze the mechanisms of probiotic treatment for SCI through the gut-spinal cord axis.

Methods: A rat model of SCI was established to evaluate the therapeutic effects of probiotics. Fecal samples were analyzed to assess gut microbiota composition and metabolite profiles, while differential gene expression in spinal cord tissue was examined.

Results: Pathological assessments demonstrated that probiotic treatment facilitated structural restoration of the spinal cord tissue. Behavioral evaluations via the Basso Mouse Scale (BMS) and inclined plane tests revealed significant improvements in locomotor recovery after SCI. Metagenomic sequencing showed that probiotics enhanced gut microbiota diversity, particularly enriching the relative abundance of Bacillota (formerly Firmicutes) and Clostridia. Metabolite profiling identified an enrichment of key tryptophan metabolites, including 3-Indoleacetonitrile, Xanthoxic acid, Serotonin, and Tryptophanol. Transcriptomic analysis identified 468 upregulated and 173 downregulated genes in spinal cord tissues. Furthermore, gut microbiota, microbial metabolites and spinal cord gene expression were integrated to construct a "gut microbiota-tryptophan metabolites-signaling pathway network" using Cytoscape v.3.10.2. This network linked 19 microbial species (17 belonging to Bacillota and Clostridia, including seven Lactobacillus species) with tryptophan metabolites and downstream signaling pathways. Among these, tryptophan metabolites activated 17 genes predominantly involved in anti-inflammatory and neuroregenerative processes. Protein-level validation confirmed the neuroprotective and anti-inflammatory effects of probiotics.

Conclusion: The "Gut microbiota-tryptophan metabolites-signaling pathway network" offers novel therapeutic targets for SCI injury treatment. Probiotics exert their effects by modulating gut microbiota and enhancing tryptophan metabolism, thereby influencing multiple signaling pathways in the spinal cord that can lead to anti-inflammatory and neuroprotective outcomes.

Keywords: Probiotic, Gut-Spinal Cord Axis, Spinal Cord Injury, tryptophan metabolism, Inflammatory Response, Neural Regeneration

Introduction

Spinal cord injury (SCI) is a severe disabling condition that results in the loss of motor, sensory, and autonomic functions, commonly causes by traffic accidents, falls, or sports injuries.[1] The incidence of SCI is increasing annually, with the mortality rate for spinal cord injuries in developed countries ranging from 3.1% to 22.2%.[2] Current clinical treatments for SCI primarily include early surgical spinal cord decompression and improvement of spinal perfusion.[3] Although these interventions have reduced the mortality rate associated with SCI, effective methods to repair SCI and

Received: 23 December 2024
Accepted: 29 May 2025
Published: 7 June 2025

Graphical Abstract

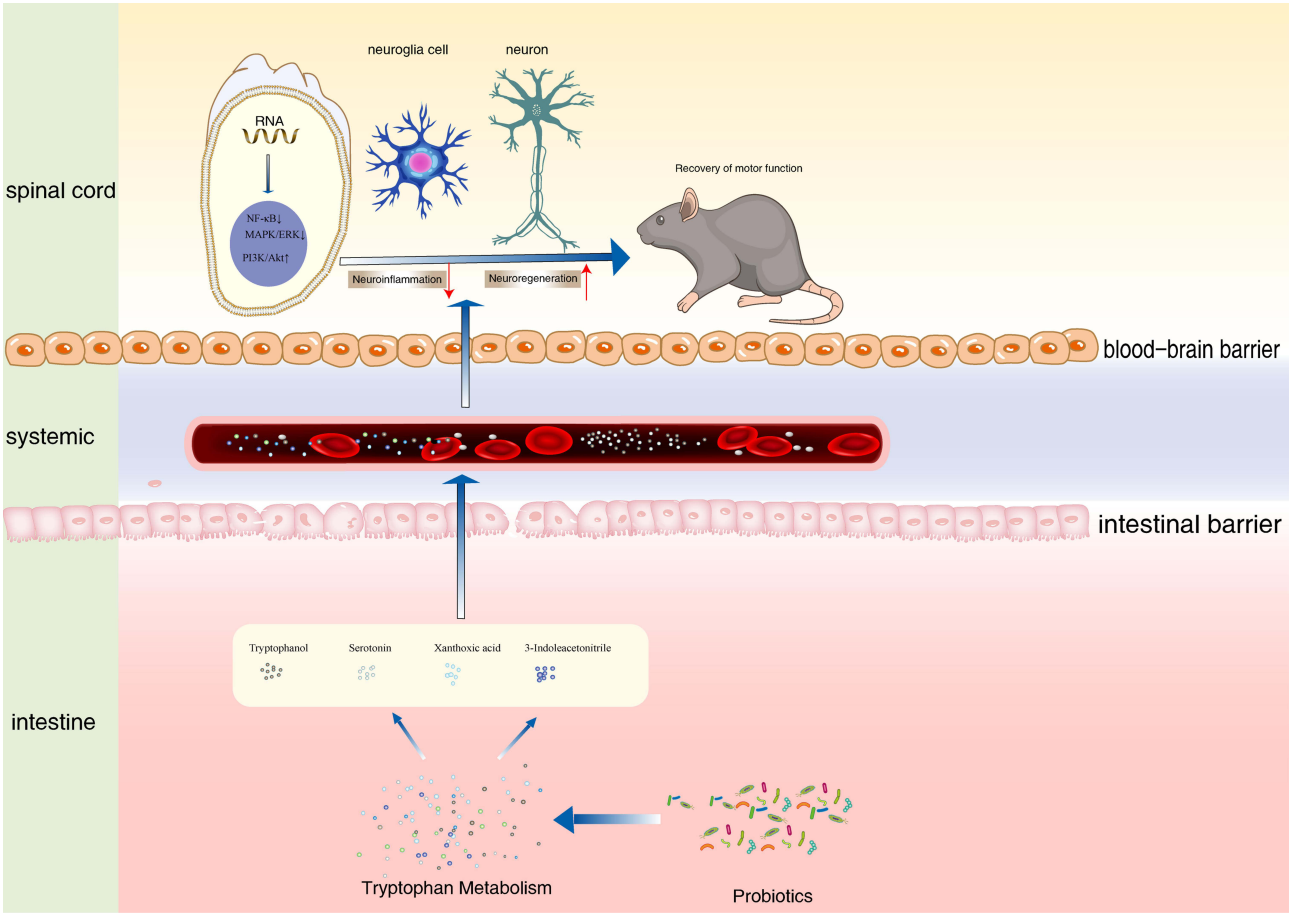

improve severe neurological dysfunction are still lacking.[4] Therefore, this study attempts to explore effective treatments for SCI by focusing on improving gut microbiota dysbiosis after SCI.

The gut microbiota is a diverse and dynamic community of microorganisms that includes beneficial, commensal, and potentially harmful bacteria. Maintaining microbial diversity and a balanced composition is crucial for supporting the host's internal ecological stability.[5–7] There is a bidirectional regulatory pathway between the gut microbiome and the central nervous system (CNS), commonly referred to as the "gut-brain axis".[8,9] Through this axis, gut microbiota can influence immune responses, which may play a role in the progression and treatment of diseases such as multiple sclerosis, Alzheimer's disease, and Parkinson's disease.[10,11] Additionally, gut microbes can produce specific metabolites that promote neural regeneration, playing a key role in treating neurodegenerative diseases.[12,13] Therefore, this study builds upon existing research highlighting the role of gut microbiota in SCI by further exploring the "gut-brain axis" and proposing the "gut-spinal cord axis" as a potential therapeutic target for SCI, which might represent a promising research direction. Studies have shown that SCI leads to an increase in inflammation-associated microbes.[14] Additionally, several studies have confirmed that improvement of gut microbiota dysbiosis could effectively repair SCI and promote the recovery of motor function after SCI.[15] However, the mechanisms that the improvement of gut microbiota disorder repairs SCI remain unclear.

This study aims to investigate how probiotics contribute to SCI treatment through the concept of the "gut-spinal cord axis". By constructing rat models, the study will evaluated the effects of probiotic treatment. Metagenomic sequencing, untargeted metabolomics analysis, and transcriptome sequencing (RNA-seq) were performed to analyze changes in the

gut microbiota, microbial metabolites, and spinal cord target genes. Based on the sequencing data, a gut microbiota-metabolite-signaling pathway network was constructed to explore the molecular mechanisms by which probiotics improve SCI through gut microbiota modulation. The findings of this study provide new potential therapeutic targets for SCI treatment.

Materials and Methods

Animals and Model Preparation

A total of 24 adult female Sprague-Dawley rats (250 ± 20 g) were housed in standard environmental conditions, with a temperature of 22 ± 2°C, humidity of 55% ± 10%, and a 12-hour light-dark cycle. The rats were provided with unrestricted access to food and water throughout the study. The animals were randomly assigned to three groups, with eight rats in each group: a sham surgery group, a spinal cord injury (SCI) group, and a VSL#3 treatment group. In the sham surgery group, rats underwent laminectomy at the T10 level without SCI induction. Rats in the SCI and VSL groups were subjected to SCI modeling. For SCI induction, animals were anesthetized with 2% isoflurane, and a T10 laminectomy was performed to expose the spinal cord. A 5 g weight was dropped from a height of 6.5 cm onto the exposed spinal cord to induce a contusive injury. After surgery, rats in the SCI group were maintained on a standard diet, while those in the VSL group received daily oral administration of VSL#3 probiotics via gavage. VSL#3 is a multi-strain probiotic, classified as a medical food, containing 8 bacterial species: Lactobacillus acidophilus, Lactobacillus plantarum, Lactobacillus paracasei, Lactobacillus delbrueckii subsp. bulgaricus, Bifidobacterium longum, Bifidobacterium breve, Bifidobacterium infantis, and Streptococcus thermophilus. The bacterial content in 1 gram of VSL#3 ranges from 112.5 billion to 900 billion colony-forming units (CFU), depending on the product formulation. On day 21 post-surgery, fresh fecal samples were collected from each rat and placed into sterile tubes for metagenomic and untargeted metabolomic analyses. The rats were then euthanized, and spinal cord tissue was harvested for subsequent RNA sequencing (RNA-seq) analysis.

Magnetic Resonance Imaging (MRI)

At 3 days post-injury, the rats underwent MRI using a Bruker 9.4T Biospec small animal MRI scanner (Bruker BioSpin, Ettlingen, Germany) equipped with a four-channel surface coil. Anesthesia was induced with 1.5% isoflurane (RWD Life Science Co., Shenzhen, China), administered via a small animal anesthesia device compatible with the MRI system. The rats were then placed on a dedicated fixation system. The imaging protocol included T1-weighted and T2-weighted sequences with the following parameters: matrix size of 320×320, slice thickness of 0.3 mm, echo time/repetition time of 24/1200 milliseconds, and flip angle of 90°. Vascular images were obtained in the sagittal plane using the Bruker ParaVision 6.0 system (Bruker, Ettlingen, Germany). Subsequently, the rats were placed on a 40°C heating pad to recover.

Hematoxylin and Eosin Staining (H&E)

Histopathological changes were observed using H&E. At 21 days post-injury, rats were anesthetized with 3% pentobarbital sodium and underwent cardiac perfusion. The T8~T10 spinal cord tissues, 5 mm above and below the injury site, were carefully collected and fixed in 4% paraformaldehyde (Solarbio, Beijing, China) at 4°C overnight. These spinal cord tissue specimens were then sectioned into 5 μm thick slices using a microtome (Leica, Wetzlar, Germany). The prepared slices were deparaffinized in xylene and different concentrations of ethanol. They were stained with hematoxylin (Solarbio) for 5 minutes, washed with water, and differentiated. The slices were dehydrated in 85% and 95% graded alcohols for 5 minutes each, stained with eosin for 5 minutes, dehydrated in graded ethanol, and then mounted in neutral gum. Representative images were observed and captured using a light microscope (BX53F2, Olympus, Tokyo, Japan).

Behavioral Tests

The motor function of rats was observed at 1 day, 1 week, 2 weeks, and 3 weeks after SCI modeling. All observations and data analysis were conducted in a double-blind manner, where the evaluators were unaware of the rat's identification

number and group assignment. Two researchers performed the functional assessments, and the final score for each rat was determined by consensus between the two researchers. In case of a disagreement, a third independent evaluator was invited to participate in the assessment. The same researchers were responsible for the entire process of functional assessment, and no personnel changes or substitutions were allowed midway.

The Basso Mouse Scale (BMS) Score was calculated as following: each rat underwent a double-blind motor function test, with hindlimb movements recorded at specified time points. The BMS score represents the recovery status of hindlimb motor function after SCI, with higher scores indicating better recovery. The scores range from 0 to 9, with 9 indicating normal motor function equivalent to that of healthy animals, and 0 indicating full loss of motor function.

The Inclined Plane Test was performed as followed: rats were placed on an inclined plane with a rubber mat. The rat's body axis was aligned parallel to the axis of the inclined plane, with the rat's head facing the higher end of the inclined plane. Starting from 0°, the angle of inclination was increased by 5° each time to observe the maximum angle at which the rat could remain on the inclined plane for 5 seconds. Each animal was tested 5 times, and the average angle was taken as the measurement value.

Metagenomics Analysis

DNA extraction and sequencing: Fecal DNA was extracted using the QIAamp DNA Stool Mini Kit (Qiagen, Germany) according to standardized protocols. Paired-end sequencing (2 × 150 bp) was performed on the Illumina NovaSeq 6000 platform. Raw sequencing reads underwent a series of processing steps to obtain quality-filtered reads for further analysis. Firstly, sequencing adapters were removed from reads using Cutadapt (v1.2.1). Secondly, low-quality reads were trimmed using a sliding-window algorithm in fastp, a FASTQ data pre-processing tool.[16] Thirdly, reads were aligned to the host rat genome using BMTagger to eliminate host contamination. Following these steps, taxonomic classifications of metagenomic sequencing reads from each sample were performed using Kraken2[17] against a RefSeq-derived database containing genomes from archaea, bacteria, viruses, fungi, protozoans, metazoans, and Viridiplantae. Reads assigned to metazoans or Viridiplantae were removed for downstream analysis. For each sample, assembly was performed using Megahit (v1.1.2)[18] with the meta-large preset parameters. Contigs longer than 200 bp were pooled and clustered using mmseqs2[19] with the "easy-linclust"mode, setting a sequence identity threshold of 0.95 and a covered residue of the shorter contig to 90%. Taxonomy of the non-redundant contigs was assigned by aligning them against the NCBI-nt database using mmseqs2 with the "taxonomy" mode, excluding contigs assigned to Viridiplantae or Metazoa from further analysis. Gene prediction in the contigs was performed using MetaGeneMark[20] with the "easy-cluster" mode, setting a protein sequence identity threshold of 0.90 and a covered residue of the shorter contig to 90%. To assess gene abundances, high-quality reads from each sample were mapped to the predicted gene sequences using Salmon in the quasi-mapping-based mode with –meta –minScoreFraction=0.55. Abundance values were normalized in metagenomes using CPM (copies per kilobase per million mapped reads). Functional annotations of the non-redundant genes were obtained by annotating them against the protein databases of KEGG, EggNOG, and CAZy using mmseqs2 with the "search" mode. EggNOG and GO annotations were obtained using EggNOG-mapper (v2),[21] while KOs were obtained using KOBAS.[22]

Untargeted Metabolomics

Fecal samples were collected immediately after defecation, flash-frozen in liquid nitrogen, and stored at −80°C until further processing. Approximately 10 mg of each sample was placed on dry ice and transferred into 2 mL Eppendorf tubes. The samples were homogenized in 200 μL of water with five ceramic beads using a tissue homogenizer. Metabolites were extracted by adding 800 μL of a methanol/acetonitrile (1:1, v/v) mixture. The resulting solution was centrifuged at 14,000g for 15 minutes at 4°C, and the supernatant was subsequently dried using a vacuum centrifuge. For LC-MS analysis, the dried samples were reconstituted in 100 μL of a solvent mixture (acetonitrile/water, 1:1, v/v). Metabolite separation was conducted using an Agilent 1290 Infinity ultra-high-performance liquid chromatography (UHPLC) HILIC column. To minimize detection variability, samples were analyzed in random order, with quality control (QC) samples included to ensure system stability and data reliability. Mass spectrometric analysis was performed on an AB Triple TOF 6600 mass spectrometer, allowing for the acquisition of both primary and secondary spectra. Raw data in Wiff format were converted to.mzXML format using ProteoWizard software. Further processing, including peak

alignment, retention time correction, and peak area extraction, was carried out using XCMS software. The processed data underwent metabolite identification, followed by data preprocessing, quality evaluation, and statistical analyses, including univariate and multivariate assessments, differential metabolite identification, correlation analysis, and pathway analysis using the KEGG database.

RNA-Seq Analysis

Total RNA was extracted using Trizol Reagent (Invitrogen Life Technologies, Carlsbad, CA, USA). The concentration, purity, and integrity of the RNA were evaluated using a NanoDrop spectrophotometer (Thermo Scientific, Waltham, MA, USA). A total of 3 μg of RNA was used as input material for the subsequent RNA sequencing library preparation. The sequencing libraries were constructed through the following steps. First, mRNA was isolated from the total RNA using poly-T oligo-attached magnetic beads. RNA fragmentation was induced by divalent cations in the presence of heat, within an Illumina proprietary fragmentation buffer. First-strand cDNA synthesis was performed using random primers and SuperScript II reverse transcriptase. Second-strand cDNA synthesis was then carried out using DNA Polymerase I and RNase H. Any remaining overhanging ends were converted into blunt ends via exonuclease and polymerase activities, and the enzymes were subsequently removed. The 3′ ends of the DNA fragments were adenylated before Illumina PE adapter oligonucleotides were ligated to the fragments in preparation for hybridization. To select cDNA fragments of the preferred 400–500 bp length, the library fragments were purified using the AMPure XP system (Beckman Coulter, Beverly, USA). DNA fragments with ligated adaptor molecules on both ends were selectively enriched using Illumina PCR Primer Cocktail in a 15-cycle PCR reaction. Products were purified using the AMPure XP system and quantified using the Agilent high sensitivity DNA assay on a Bioanalyzer 2100 system (Agilent, La Jolla, USA). The sequencing library was then sequenced on the NovaSeq 6000 platform (Illumina, San Diego, USA) by Shanghai Personal Biotechnology Co. Ltd.

Multi-Omics Analysis and Network Construction

Based on the changes of gut microbiota, gut microbiota metabolites, and genetic changes between the SCI group and the VSL group, the gut-spinal cord axis: the gut microbiota-metabolite-signaling pathway network was constructed by multi-omics analysis to analyze the mechanism of repairing SCI. Correlations between these datas were calculated, with significant correlations defined as $|r| > 0.8$ and $p < 0.05$. These correlations formed the edges in the network, while nodes represented microbial genera, metabolites, and differentially expressed genes. The network was visualized using Cytoscape (3.10.2), with node sizes and colors reflecting their connectivity and type. The network layout was optimized for readability, and key hubs and interactions were explored to understand the "gut-spinal cord axis."

Western Blot (WB)

Total protein from rat spinal cord tissue was extracted using RIPA lysate (P0013B, Beyotime, Shanghai, China). Proteins were separated by SDS-PAGE and transferred onto a nitrocellulose membrane. The membrane was blocked with 5% skim milk for 90 minutes to prevent non-specific binding. The membranes were then incubated overnight at 4°C with primary antibodies against p-Akt, Akt, p-P65, P65, p-Erk1/2, Erk1/2, and GAPDH. After primary antibody incubation, the membranes were incubated with HRP-conjugated secondary antibodies [HRP anti-mouse (AWS0001a) and HRP anti-rabbit (AWS0002a), both 1:5,000, Abiowell, Changsha, China] at room temperature for 90 minutes. Protein bands were visualized using SuperECL Plus (K-12045-D50, Advansta, San Jose, USA) and photographed using a Chemiscope6100 (CLiNX, Shanghai, China). GAPDH was used as the internal reference.

Statistical Analysis

Based on the taxonomic and functional profiles of non-redundant genes, linear discriminant analysis effect size (LEfSe) was performed to detect differentially abundant taxa and functions across groups using the default parameters.[23] Beta diversity analysis was performed to investigate the compositional and functional variation of microbial communities across samples using Bray-Curtis distance metrics and visualized via principal coordinate analysis (PCoA), nonmetric multidimensional scaling (NMDS), and unweighted pair-group method with arithmetic means (UPGMA) hierarchical clustering.[24] Western blot data were analyzed using unpaired Student's *t*-test for two-group comparisons or one-way

ANOVA followed by Tukey's post-hoc test for multiple-group comparisons. Behavioral test data were analyzed using two-way repeated-measures ANOVA with Bonferroni correction to assess group differences over time. Metabolomics data were analyzed using univariate and multivariate statistical methods after preprocessing with XCMS software. Normality of the data was assessed using the Shapiro–Wilk test before parametric tests were applied. All statistical analyses were performed using GraphPad Prism 9.0 and R software, and results were considered statistically significant at $P < 0.05$.

Results

The Therapeutic Effects of Probiotics

In the sham surgery (Sham) group, SCI group, and VSL (SCI+VSL#3) group, sagittal T1- and T2-weighted images were obtained using an MRI scanner 3 days post-operation (Figure 1A). Spinal cord MRI revealed a T1 hypointense area and a T2 hyperintense area at the surgical site, indicating successful modeling of SCI. At 21 days post-injury, cross sections of the rat spinal cord were collected and subjected to H&E to observe histopathological changes. The sham group exhibited intact spinal cord structures without hemorrhage, necrosis, or inflammatory cell infiltration. In contrast, the SCI group showed disrupted spinal cord architecture with hemorrhage, inflammatory cell infiltration, and neuronal loss. The VSL group demonstrated spinal cord repair with the recovery of spinal cord morphology and only a few scabs are still healing (Figure 1B). According to BMS score and inclined plane test, the study found that the SCI group exhibited

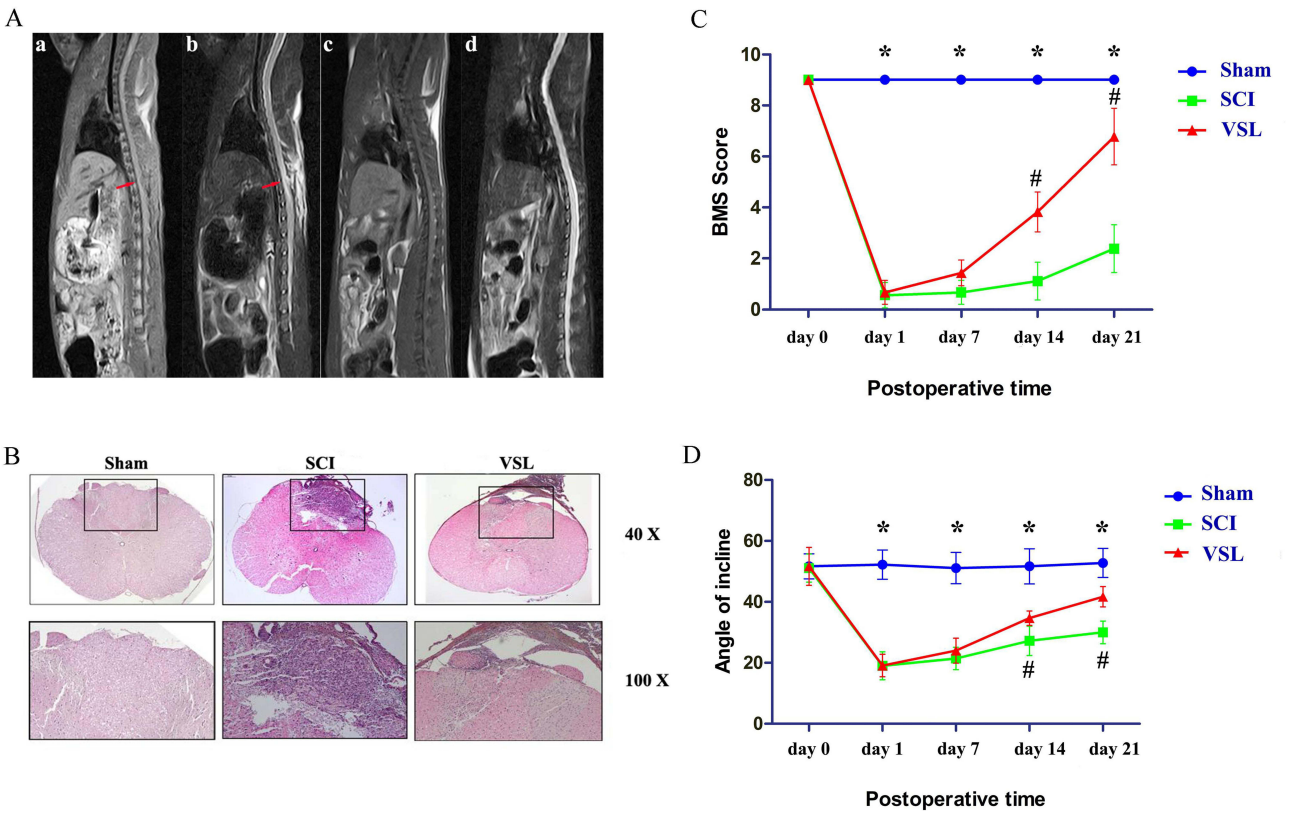

Figure 1 Imaging, histopathological, and behavioral changes in the rat model of SCI. (**A**) MRI images of sagittal sections of the rat spinal cord showing T1W MRI and T2W MRI at 3 days. MRI of the SCI group shows a T1 hypointense area and a T2 hyperintense area at the injury site. Red arrows indicate abnormal signal areas around the impact point of the spinal cord (a, b). T1W MRI and T2W MRI of the sham group show intact spinal cord tissue (c, d). (**B**) The images of H&E of across sections of the rat spinal cord at 21 days. Compared to the sham group, the other two groups exhibit varying degrees of hemorrhage, cavitation, necrosis, and inflammatory cell infiltration. The SCI group shows a noticeable blood scab on the spinal cord surface and significant tissue damage at 21 days, whereas the SCI+VSL#3 group shows good recovery with almost restored spinal cord morphology and minimal blood scabs on the surface still healing. (**C**) Behavioral monitoring assessed by Basso Mouse Scale (BMS) scores and (**D**) inclined plane test. On the first day post-operation, both the SCI and SCI+VSL#3 groups suffered the same degree of SCI. Over time, the injuries gradually recovered, with the SCI+VSL#3 group showing better recovery in both tests. Data are expressed as $x \pm s$, $n = 8$ rats for each group. *: Statistically significant compared to the sham group, $P < 0.05$; #: Statistically significant compared to the SCI group, $P < 0.05$.

significant motor function impairment, while the administration of probiotics significantly improved motor function recovery in the rats with SCI (Figure 1C and D).

The Effects of SCI and Probiotics on Gut Microbial Composition

To investigate the effect of probiotics on the gut microbiota of rats, fecal samples were subjected to metagenomic sequencing to compare the microbiota composition of the sham-operated group (n = 8), SCI group (n = 8), and VSL group (n=8). Alpha diversity indices were used to compare microbial richness. As shown in Figure 2A, compared to the sham group, the Chao1 index, ACE index, and Observed species index were significantly decreased in both the SCI group and the VSL group. The rarefaction curve showed clear asymptotes in all three groups (Figure 2B), Good's coverage index is close to 1, which indicated that the sequencing data was reasonable. Beta-diversity analysis was conducted based on Bray-Curtis dissimilarity. The results of PCoA analysis showed significant differences in bacterial colony composition among the samples of the SCI group, the sham-operated group, and VSL group (Figure 2C). These results indicated that SCI significantly reduced gut microbiota diversity in rats.

Based on the species annotation results, the top ten species of various groups were selected at the genus level (Figure 3A). We found that *Enterenecus, UBA3282, Lawsonibacter, Pelethomonas, Ligilactobacillus, COE1,*

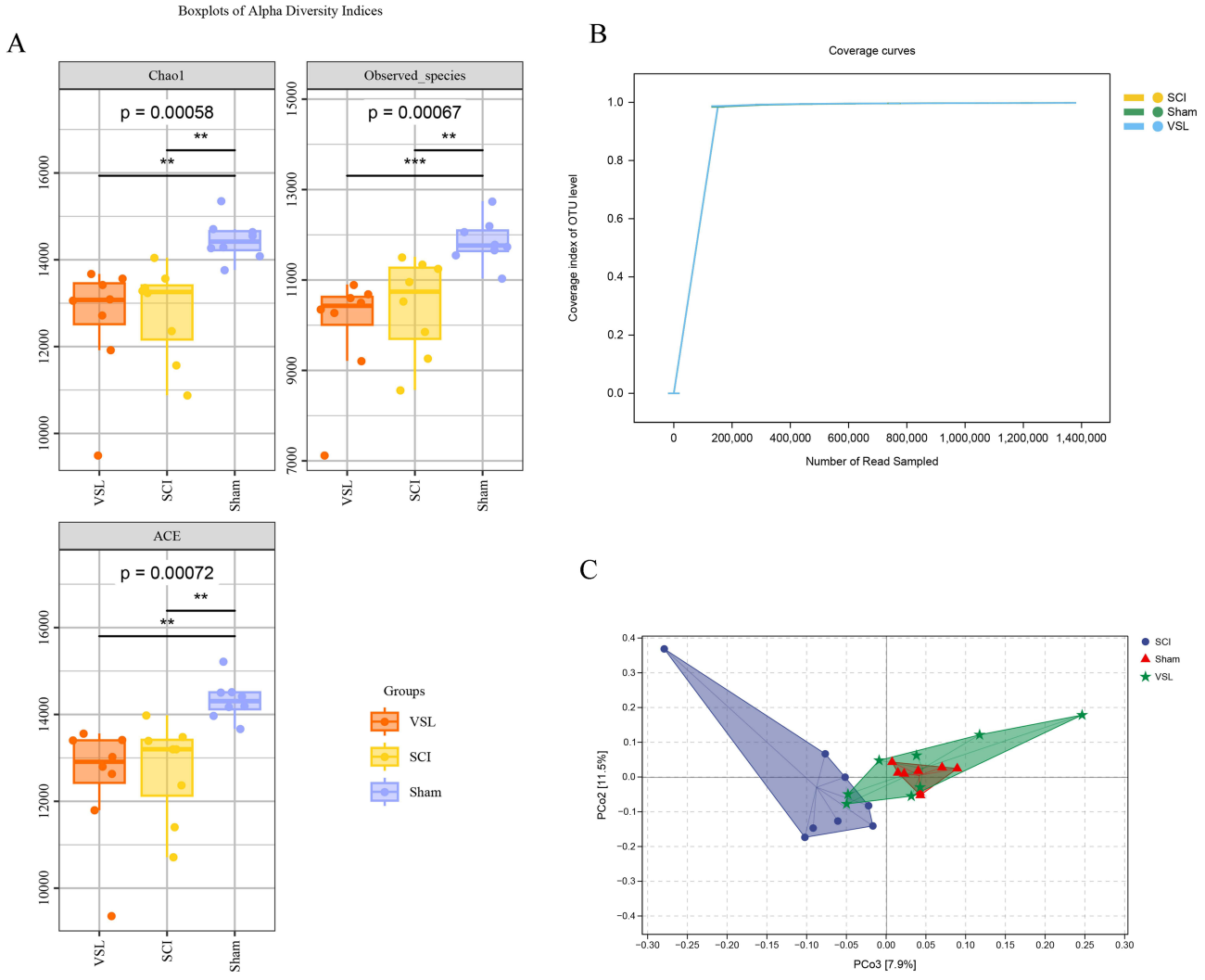

Figure 2 α-Diversity and β-Diversity of the gut microbiota. (**A**) α-Diversity analysis using Kruskal–Wallis rank sum test with Dunn's test for post-hoc analysis (Chao1 index, ACE index, Observed species index). (**B**) Rarefaction curves depict microbial diversity in intestinal samples from three groups, showing the number of observed taxa with increasing sequencing depth. (**C**) β-Diversity analysis based on Bray-Curtis distance. n = 8 rats for each group. **: P < 0.01; ***: P < 0.001.

https://doi.org/10.2147/JIR.S513900

https://doi.org/10.2147/JIR.S513900

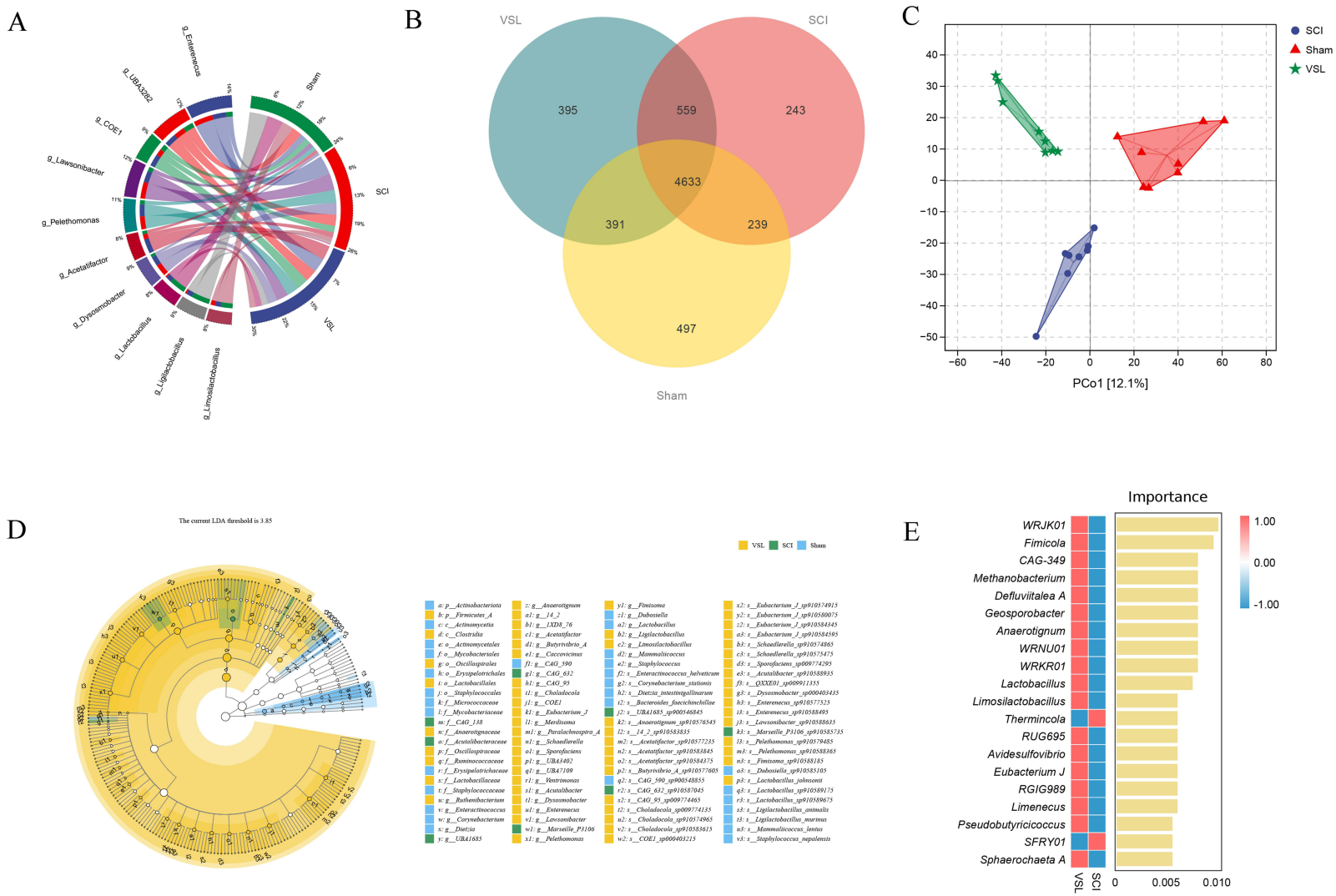

Figure 3 Changes in gut microbiota composition after SCI. (**A**) Circos plot showing the taxonomic composition at the genus level of the gut microbiota (n=8 per group). (**B**) Venn diagram displaying the number of shared and unique gut microbiota among different groups. (**C**) Partial least squares discriminant analysis (PLS-DA) of rat gut microbiota for dimensionality reduction. (**D**) LEfSe generated cladogram to identify bacterial taxa with significant differences between groups. The diameter of each node is proportional to the relative abundance of that taxon (LDA > 3.85 and P < 0.05). (**E**) Random forest analysis at the genus level. n = 8 rats for each group.

Dysosmobacter, Lactobacillus, Acetatifactor, and *Limosilactobacillus* were dominant in all rat gut microbiomes. Comparatively, the abundance of *Lactobacillus, Acetatifactor, Limosilactobacillus*, and *Ligilactobacillus* in the SCI group was significantly lower than that in the sham group. However, after the application of probiotics, the abundance of these genera increased significantly.

To study common and unique species across rat groups, we performed community analysis using a Venn diagram (Figure 3B). The diagram showed 4633 shared amplicon sequence variants (ASVs) among the three groups, with 497 unique ASVs in the sham group, 243 in the SCI group, and 395 in the VSL group. Both the sham and VSL groups contained more unique ASVs than the SCI group. PLS-DA revealed significant differences in bacterial community composition between the groups (Figure 3C). Linear discriminant analysis (LDA) identified significant differences in bacterial taxa at all taxonomic levels ($P<0.05$, LDA>3.85; Figure 3D). Specifically, probiotics led to significant changes in the VSL group, including increased abundance of Bacillota (formerly Firmicutes) (phylum), Clostridia (class), Oscillospirales and Lachnospirales (order), and Anaerotignaceae, Oscillospiraceae, Ruminococcaceae, and Lachnospiraceae (family). At the genus and species levels, the VSL group showed greater species richness, suggesting that these microbiota changes may affect the host in various ways. Random forest analysis identified key marker species driving group differences, with dominant strains in the VSL group including *Fimicola, Methanobacter, Geosporobacter, Anaerotignum, Lactobacillus*, and *Limosilactobacillus* (Figure 3E), indicating that probiotics can improve the microbiota composition in SCI rats.

The Effects of SCI and Probiotics on Gut Microbiota-Derived Metabolites

To investigate the effect of probiotics on the gut metabolism of SCI rats, we used a non-targeted metabolomic approach. After characterizing the metabolites, principal component analysis (PCA, Figure 4A) and partial least squares discriminant analysis (PLS-DA, Figure 4B) were performed. PCA revealed significant metabolic differences (PC1: 15.1%, PC2: 13.4%, R2X= 0.53). PLS-DA showed strong separation between the sham, SCI, and VSL groups (R2X= 0.475, R2Y= 0.992, Q2= 0.84). The volcano plot indicated that in the VSL group, 376 metabolites were significantly decreased, and 658 were increased (Figure 4C). A heatmap of 132 metabolites from fecal screening showed significant differences between the sham and SCI groups, with probiotic treatment partially reducing these differences (Figure 4D). These results suggest that SCI-induced changes in gut metabolism can be reversed by probiotics.

Subsequently, KEGG pathway enrichment analysis was applied to the differential metabolites, selecting the top 20 pathways with the lowest p-values for enrichment display (Figure 4E). The KEGG pathway enrichment analysis revealed that the two primary metabolic pathways regulated by probiotics are Arachidonic acid metabolism and Tryptophan metabolism. The Rich Factor represents the ratio of the number of differential metabolites enriched in a pathway to the total number of differential metabolites annotated within that pathway. A higher Rich Factor indicates a greater degree of enrichment. Among the significantly upregulated pathways, Arachidonic acid metabolism, Tryptophan metabolism, Phenylalanine metabolism, Prodigiosin biosynthesis, and Caprolactam degradation exhibited the highest levels of enrichment (Figure 4F). Random forest analysis indicated that 3-Indoleacetonitrile, belonging to the tryptophan metabolic pathway, had the highest feature importance value (Figure 5A), underscoring the critical role of tryptophan metabolism in model predictions and suggesting that this pathway may play a significant role in the therapeutic mechanisms for SCI. Furthermore, we conducted a metabolomic analysis targeting tryptophan to elucidate the regulatory effects of probiotics on tryptophan metabolism. As illustrated, SCI significantly reduced the levels of 3-Indoleacetonitrile, Indoleacetaldehyde, Xanthoxic acid, and Tryptophanol in the gut, whereas the administration of probiotics restored the concentrations of these tryptophan derivatives (Figure 5B–E). Additionally, probiotics increased the levels of Tryptamine, Serotonin, and 3-Geranylgeranylindole in the gut (Figure 5F–H). These metabolites, which are part of the tryptophan indole metabolic pathway, are closely associated with inflammation and immune regulation.[25]

The Effects of SCI and Probiotics on Gene Expression

Transcriptome analysis was performed on samples from the three groups to quantify changes in gene expression. PCA based on PC1 clearly separated the samples from the sham-operated group, the SCI group, and the VSL group, with PC1 contributing to 99.1% of the variation, making it the major component (Figure 6A). Compared to the SCI group, the

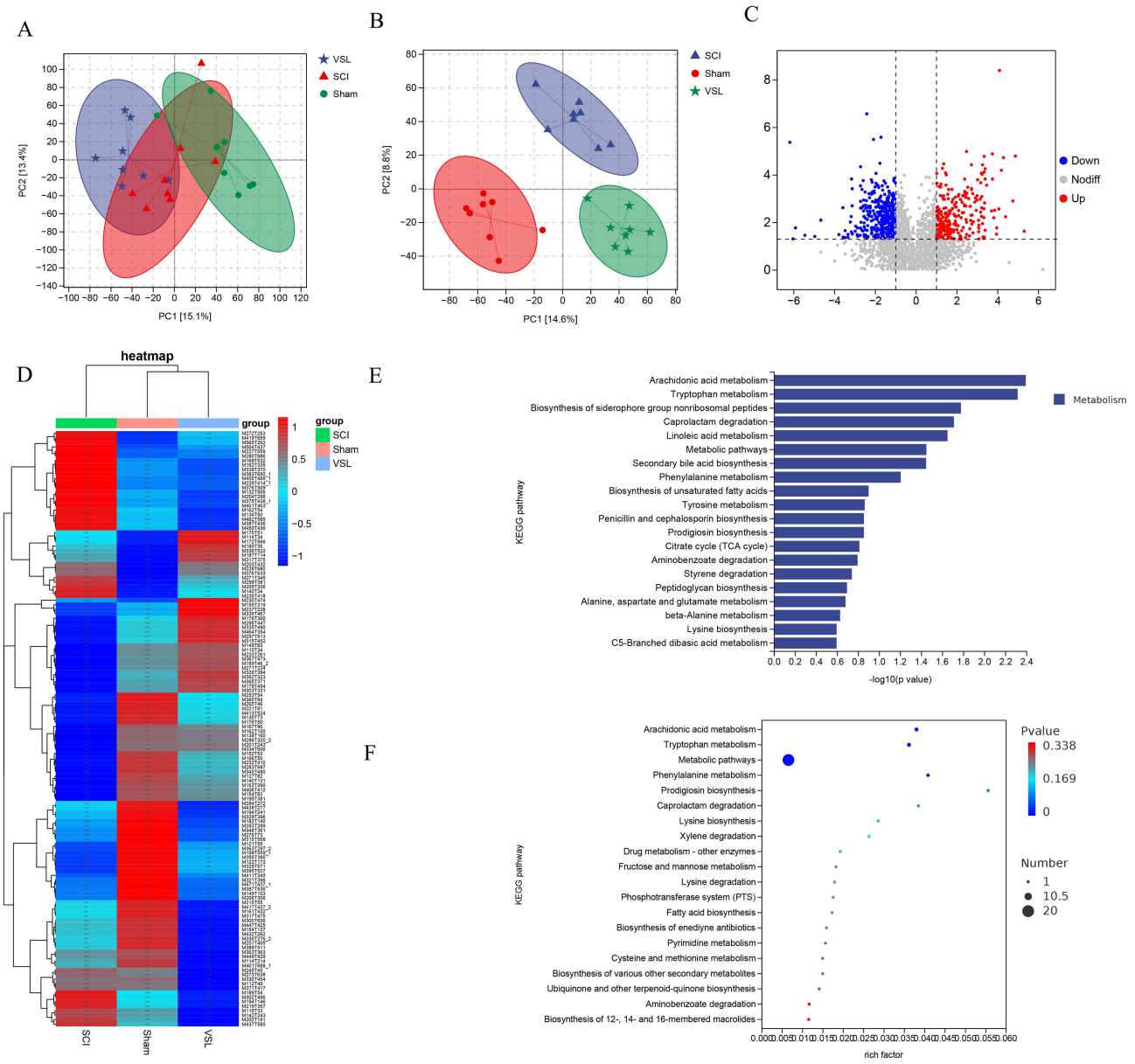

Figure 4 Selection of differential microbial metabolites after SCI and probiotic administration. (**A**) Principal component analysis (PCA) (R2X= 0.565). (**B**) Partial least squares discriminant analysis (PLS-DA) (R2X= 0.475, R2Y= 0.992, Q2 = 0.84). (**C**) Volcano plot of differential metabolites (VIP > 1.0, fold change > 1 / < −1). (**D**) Cluster analysis of differential metabolites. (**E** and **F**) KEGG pathway enrichment analysis showing that the selected differential metabolites are enriched in metabolic pathways. The size of the bubbles represents the number of different metabolites enriched in each pathway. The color of the bubbles represents the P-value of each pathway. n = 8 rats for each group.

volcano plot showed that there were 468 genes significantly increased and 173 genes significantly decreased in the spinal cord of rats in the VSL group (Figure 6B). GO functional enrichment analysis indicated significant enrichment of multiple pathways associated with insulin-like growth factor signaling and growth factor complexes (Figure 6C). This suggests that VSL may promote the repair and regeneration of SCI by regulating cellular proliferation. Moreover, KEGG pathway enrichment analysis revealed significant enrichment in several pathways within the treatment group, including those related to mineral absorption, cellular senescence, Cushing's syndrome, proximal tubular reabsorption, autoimmune diseases, graft rejection, antigen processing and presentation, and the p53 signaling pathway (Figure 6D). These pathways encompass critical mechanisms involved in mineral metabolism, cellular aging, immune and inflammatory regulation, metabolic modulation, viral infection response, and apoptosis. This indicates that probiotic treatment may

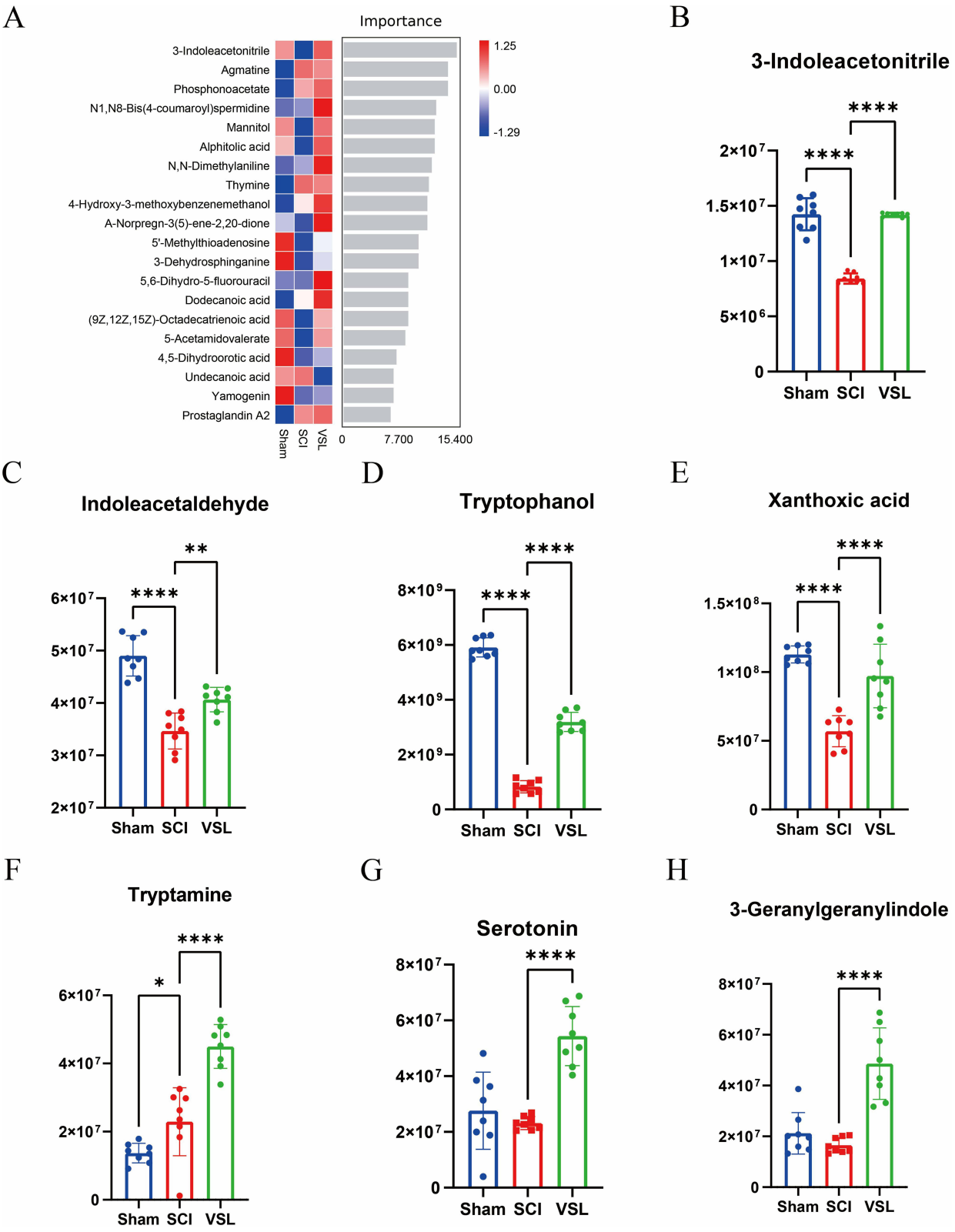

Figure 5 Key differential tryptophan metabolites regulated by VSL#3. (**A**) Random forest analysis of intestinal metabolites. From top to bottom, the importance of metabolites to the model decreases in order; These highly important metabolites can be considered as marker metabolites for inter group differences. (**B**) 3-Indoleacetonitrile, (**C**) Indoleacetaldehyde, (**D**) Tryptophanol, (**E**) Xanthoxic acid, (**F**) Tryptamine, (**G**) Serotonin, (**H**) 3-Geranylgeranylindole. The data were expressed as the mean ± SD, and were analyzed by one-way ANOVA. n = 8 rats for each group. *p < 0.05; **p < 0.01; ****p < 0.0001.

https://doi.org/10.2147/JIR.S513900

https://doi.org/10.2147/JIR.S513900

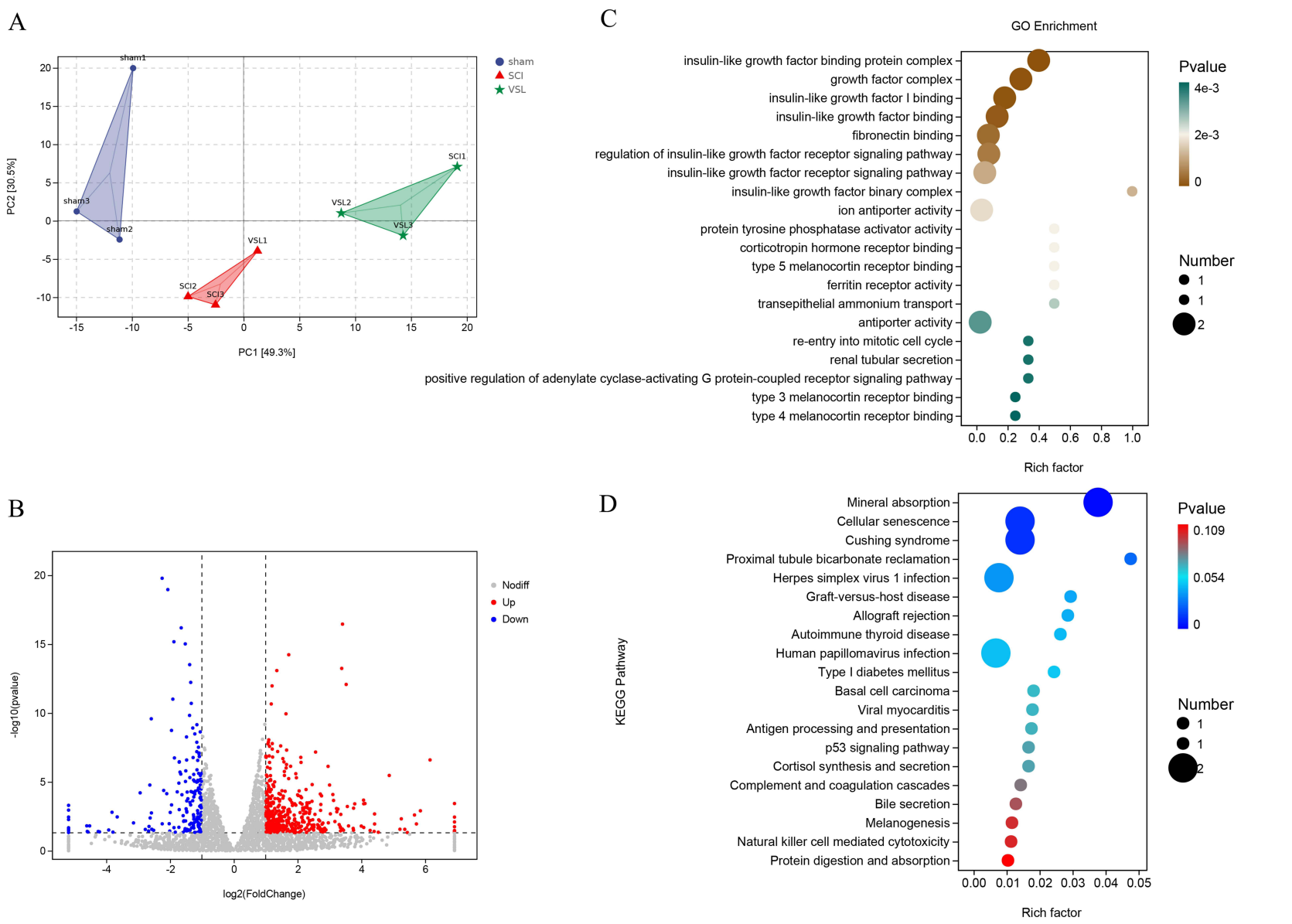

Figure 6 RNA-seq Analysis of Spinal Cord-Related Gene Expression. (**A**) PCA plots of the three sample groups. (**B**) Differential expression analysis between the SCI and VSL groups ($P < 0.05$) (VIP > 1, log2(FoldChange) > 1/-1). (**C**) GO functional enrichment analysis between the SCI and VSL groups. (**D**) KEGG pathway enrichment analysis between the SCI and VSL groups. The size of the bubbles represents the number of different metabolites enriched in each pathway. The color of the bubbles represents the P-value of each pathway. n = 3 rats for each group.

regulate metabolic homeostasis through multiple pathways, enhance immune function, and improve the repair and regeneration of SCI.

Network Was Established by Multi-Omics Analysis

A visual integration network of the "gut microbiota-metabolites-signaling pathway" was constructed using Spearman correlation analysis (Figure 7A). The differential microbiota, metabolites, and KEGG enrichment analysis results from the SCI group and the VSL group were imported into Cytoscape v.3.10.2. This software facilitated the integration of the relationships between gut microbiota, metabolites, and spinal cord signaling pathways, culminating in the formation of the "gut microbiota-metabolites-signaling pathway network". As previously demonstrated, the tryptophan metabolic pathway is a principal metabolic pathway influenced by probiotics; therefore, we refined this network axis based on tryptophan metabolites. The core metabolites identified, which were significantly increased in the VSL group, included 3-Indoleacetonitrile, Xanthoxic acid, Serotonin, and Tryptophanol. According to the correlation network, the administration of probiotics resulted in a significant increase in 19 microbial species producing these metabolites (eg, *Limosilactobacillus reuteri, Parabacteroides distasonis*, and *Lactobacillus johnsonii*), while seven species exhibited significant decreases (eg, *Duncaniella freteri*). Moreover, these tryptophan derivatives upregulated the expression of 17

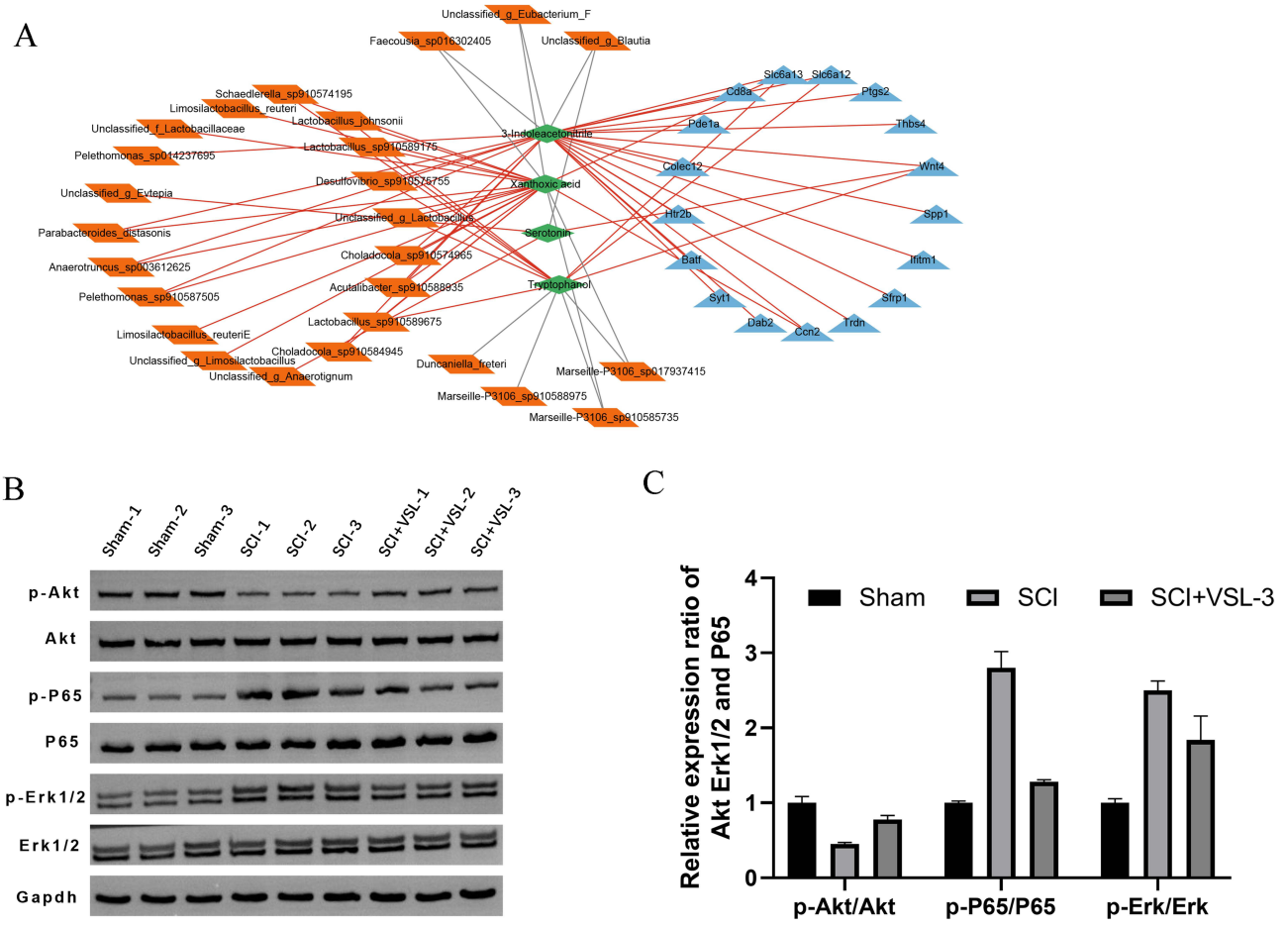

Figure 7 Network of Significant Interactions between Gut Microbiota, Gut Microbiota Metabolites, and Genes. (**A**) The relevant network consists of 26 bacteria, 4 tryptophan metabolites, and 17 pairs of regulatory genes. The Orange parallelogram represents the gut microbiota, the green diamond represents the corresponding tryptophan metabolites of the microbiota, and the blue triangle represents the target genes. The red and gray lines represent positive and negative correlations, respectively, with parameters set to | r |>0.8 and p<0.05. (**B**) Western blotting analysis showing the effect of probiotics on the NF-κB, MAPK/ERK, and PI3K/Akt signaling pathways in SCI rats. (**C**) Relative expression ratio of Akt, Erk1/2 and P65. Compared to the sham group, the expression levels of p-Akt are significantly decreased, while the expression levels of p-P65 and p-Erk1/2 are significantly increased in the SCI group. Compared to the SCI group, treatment with probiotics (VSL#3) significantly upregulates the expression of p-Akt and significantly downregulates the expression of p-P65 and p-Erk1/2. GAPDH is used as an internal reference to ensure consistency in protein loading. Data are expressed as x ± s, n = 3 rats for each group.

https://doi.org/10.2147/JIR.S513900

Table 1 Information of Target Genes in the Network Diagram

Gene Name	Protein Name	Signalling Pathway	Regulation
Spp1	Secreted phosphoprotein 1	PI3K-Akt signaling pathway, Apelin signaling pathway	Up Regulation
Thbs4	Thrombospondin 4	PI3K-Akt signaling pathway, Phagosome	Up Regulation
Wnt4	Wnt family member 4	Wnt signaling pathway, mTOR signaling pathway	Up Regulation
Sfrp1	Secreted frizzled-related protein 1	Wnt signaling pathway	Up Regulation
Trdn	Triadin	Calcium signaling pathway	Up Regulation
Pde1a	Phosphodiesterase 1Aphosphodiesterase 1A	Calcium signaling pathway	Up Regulation
Htr2b	5-hydroxytryptamine receptor 2B	Inflammatory mediator regulation of TRP channels, Serotonergic synapse, Gap junction, Neuroactive ligand-receptor interaction, Calcium signaling pathway	Up Regulation
Dab2	DAB adaptor protein 2	Endocytosis	Up Regulation
Colec12	Collectin sub-family member 12	Phagosome	Up Regulation
Ptgs2	Prostaglandin-endoperoxide synthase 2	Serotonergic synapse, VEGF signaling pathway	Up Regulation
Cd8a	CD8a molecule	T cell receptor signaling pathway, Antigen processing and presentation	Up Regulation
Ifitm1	Interferon induced transmembrane protein 1	B cell receptor signaling pathway	Up Regulation
Syt1	Synaptotagmin 1	Synaptic vesicle cycle	Up Regulation
Slc6a12	Solute carrier family 6 member 12	Synaptic vesicle cycle, GABAergic synapse	Up Regulation
Slc6a13	Solute carrier family 6 member 13	Synaptic vesicle cycle, GABAergic synapse	Up Regulation
Batf	Basic leucine zipper ATF-like transcription factor	PD-L1 expression and PD-1 checkpoint pathway in cancer	Up Regulation
Ccn2	Cellular communication network factor 2	Apelin signaling pathway	Up Regulation

genes, which, through KEGG pathways, are involved in the activation of multiple signaling pathways, including the PI3K-Akt signaling pathway, Wnt signaling pathway, mTOR signaling pathway, Calcium signaling pathway, and the regulation of TRP channels by inflammatory mediators (Table 1). The activation of these signaling pathways is associated with various biological processes, such as cell proliferation, survival, and inflammation regulation, potentially contributing to the suppression of inflammation and the repair of nerve damage following SCI. In summary, the activation of these signaling pathways may represent a potential mechanism through which VSL facilitates the repair of SCI.

The Western blot (WB) analysis results are presented in Figure 7B and C. In the sham group, the baseline levels of p-Akt, p-P65, and p-Erk1/2 were relatively low. In contrast, the SCI group showed a marked reduction in p-Akt expression, while p-P65 and p-Erk1/2 levels were significantly elevated. These findings suggest that SCI induction led to the upregulation of the NF-κB and MAPK/ERK signaling pathways, alongside the suppression of the PI3K/Akt pathway. In the SCI+VSL#3 group, a notable increase in p-Akt expression was observed compared to the SCI group, while p-P65 and p-Erk1/2 expression levels were significantly lower. These results further support the hypothesis that probiotics promote SCI recovery by enhancing the PI3K/Akt pathway and inhibiting the NF-κB and MAPK/ERK signaling cascades.

Discussion

Probiotics have demonstrated promising therapeutic effects for SCI in our study. Cross sections of the rat spinal cord after H&E staining showed the recovery of spinal cord morphology in the VSL group. According to the BMS score and inclined plane test, the study also found that the VSL group exhibited motor function recovery. Previous studies have shown that SCI affects the types and composition of gut microbiota,[26–34] our study also demonstrated that SCI could lead

to a decrease in gut microbiota diversity. After the application of probiotics, both the gut microbiota diversity and probiotics abundance increased significantly, meanwhile, some specific metabolites and gene expression also changed in our study. These results above implied that probiotics might improve intestinal flora imbalance and up-regulate specific intestinal microbial metabolites, which in turn regulate gene expression — possibly contributing to the repair of SCI. Based on the changes in the gut microbiota, microbial metabolites, and gene expression, the gut-spinal cord axis: the gut microbiota-metabolite-signaling pathway network was constructed by multi-omics analysis to analyze the mechanism of repairing SCI by probiotics.

Metabolites produced by the gut microbiota serve as a bridge between the gut microbiome and the central nervous system.[34] Research indicates that these metabolites can enter the bloodstream and spinal cord through various pathways, thereby influencing recovery from SCI.[14,35] This study identifies tryptophan metabolism as a key metabolic pathway involved in the VSL-mediated repair of SCI, based on differential metabolite enrichment analysis and random forest model predictions. Tryptophan is an essential amino acid that cannot be synthesized by the human body and must be obtained through dietary sources.[36] Notably, a significant portion of ingested tryptophan is metabolized into bioactive compounds, primarily produced by the gut microbiota.[37,38] The gut microbiota plays a crucial role in regulating tryptophan metabolism and directing its catabolism towards the production of bioactive compounds that affect immune function, metabolism, and neurotransmission.[39] This study utilized Cytoscape v.3.10.2 to integrate gut microbiota, microbial metabolites, and spinal cord gene expression, constructing a "gut microbiota-metabolites-signaling pathway network". Given that the primary metabolic pathway identified is tryptophan metabolism, we further refined this to the "gut microbiota-tryptophan metabolites-signaling pathway network", highlighting 3-Indoleacetonitrile, Xanthoxic acid, Serotonin, and Tryptophanol as key tryptophan metabolites.

Based on metagenomic sequencing, this study found that probiotic use altered the diversity of the gut microbiota, specifically increasing the abundance of Bacillota (at the phylum level), Clostridia (at the class level), Oscillospirales and Lachnospirales (at the order level), as well as Anaerotignaceae, Oscillospiraceae, Ruminococcaceae, and Lachnospiraceae (at the family level). Within the "gut microbiota-tryptophan metabolites-signaling pathway network", 17 of the 19 gut microbes positively correlated with the tryptophan metabolic pathway were found to belong to the Bacillota and Clostridia. Reports by Tian et al[40] have established a "Bacillota-SCFAs-GP metabolism-tryptophan pathway", indicating that 5-HT may serve as a mediator through which Bacillota regulate brain function. This supports the correlation observed in our study between Bacillota and the tryptophan metabolic pathway. Additionally, multiple studies have shown that members of the Clostridia enhance the metabolic capacity for tryptophan, promoting its conversion into bioactive metabolites.[41–43] The increased abundance of these microorganisms across various taxonomic levels may influence the host's systemic response by modulating tryptophan metabolism. Existing research indicates that tryptophan can be metabolized into various indole derivatives by aromatic amino acid aminotransferases (ArATs), which are stable in some *Lactobacillus* species.[44] Consistent with this, the administration of probiotics resulted in a significant increase in the abundance of six *Lactobacillus* species that produce indole derivatives, including *Limosilactobacillus reuteri, Lactobacillus johnsonii*, and others. It has been reported that *Lactobacillus* species can indirectly enhance colonic serotonin synthesis by increasing TPH1 expression.[45–47] Extensive studies have confirmed that indole metabolites produced by *Limosilactobacillus reuteri* possess antioxidant and neuroprotective properties, protecting neurons by reducing oxidative stress and inflammation-mediated damage.[37,48] Additionally, *Lactobacillus johnsonii* contributes to the generation of indole derivatives, which not only play a role in regulating host immune responses but are also associated with the synthesis of neurotransmitters such as serotonin.[49,50] Furthermore, research has indicated that *Lactobacillus johnsonii* exerts neuroprotective effects against anxiety and depression-like behaviors in stressed mice through the modulation of tryptophan metabolism.[51] Collectively, these findings suggest that the use of VSL probiotics significantly influences the microbiota-tryptophan axis by modulating the composition of the gut microbiota.

It is noteworthy that tryptophan metabolism is not only closely linked to the gut microbiota but also plays a critical role in neuroregulation.[38] Research indicates that tryptophan metabolites derived from the microbiota can influence the central nervous system by activating aryl hydrocarbon receptors (AhR) in astrocytes.[52] AhR acts as an upstream regulatory factor that can initiate the expression of multiple genes and mediate a range of responses.[53] For instance, it plays a significant role in modulating various signaling pathways related to neuroinflammatory responses and the

regeneration and repair of neural cells.[54–56] Through transcriptomic analysis and results from the "gut microbiota-tryptophan metabolites-signaling pathway network", this study discovered that tryptophan derivatives can upregulate the expression of 17 genes, thereby activating multiple signaling pathways, including the PI3K-Akt, Wnt, and mTOR pathways. The activation of these pathways is involved in several biological processes such as cell proliferation, survival, and inflammation regulation, which may be closely related to the suppression of inflammation and the repair of SCI. Reportedly, tryptophan absorbed by intestinal epithelial cells can directly activate the mTOR pathway of intracellular tryptophan receptors through a PI3K/AKT-independent mechanism.[57] Simultaneously, the PI3K/AKT/mTOR pathway, as a pro-survival signaling pathway, is activated to promote endothelial cell survival, reduce neuronal damage, minimize inflammation-induced cell death, and block neuronal injury, thereby exerting protective effects on nerve cells.[58] Furthermore, Wnt/mTOR signaling can regulate neural stem cell proliferation, differentiation, axonal regeneration, and neuroinflammation, contributing to the repair of SCI.[59] The regulation observed at the gene level suggests that tryptophan metabolism may possess extensive regulatory potential during the repair process following SCI. However, the validation results at the protein level reveal dynamic feedback regulatory characteristics of specific pathways. Notably, while the PI3K-Akt pathway is significantly activated, the MAPK/ERK and NF-κB signaling pathways are found to be suppressed. This outcome suggests that although tryptophan metabolic pathways can upregulate the expression of genes associated with pro-survival pathways such as PI3K-Akt, their activation may exert negative feedback inhibition on NF-κB and MAPK/ERK pathways, thereby reducing neuroinflammatory responses. This dynamic regulatory mechanism may provide a unique modulatory framework for neuroprotection and inflammation control in SCI, indicating that tryptophan metabolites may have multifaceted roles in the repair process.

In summary, this study provides new insights into probiotic therapy for SCI by analyzing the correlation among gut microbiota, characteristic microbial metabolites and signaling pathways. The therapeutic mechanism of probiotics for SCI can be explored through multi-omics analysis of gut microbiota, gut microbiota metabolites and RNA-seq. Based on the sequencing data, we constructed the "gut-spinal cord axis": Probiotic (e.g., Limosilactobacillus reuteri) - Tryptophan Metabolites (e.g., 3-Indoleacetonitrile) - Signaling Pathway Network (e.g., PI3K-Akt signaling pathway), which support the potential mechanisms of probiotic therapy for SCI: inhibiting spinal cord inflammation and promoting nerve repair. This comprehensive regulatory strategy in treatment approaches is innovative. This approach elucidates the multi-component and multitarget mechanisms of probiotics in treating SCI, contributing to a comprehensive understanding of the effects and mechanisms of probiotic therapy for patients with SCI. However, our study has several limitations. In future sequencing experiments, more samples need to be included. Additionally, in human studies, the specific effects of probiotics on gut microbiota and SCI are unclear. Future research and clinical trials can further explore the mechanisms of these pathways and evaluate the effectiveness and potential risks of probiotic therapy in clinical applications.

Data Sharing Statement

All data generated or analyzed during this study are included in this published article.

Ethics Approval and Consent to Participate

All animal procedures were conducted in accordance with the Regulations for the Administration of Affairs Concerning Experimental Animals (Revised by the State Council of the People's Republic of China, 2017) and the Guidelines for the Care and Use of Laboratory Animals issued by the Chinese Association for Laboratory Animal Sciences. The study was approved by the Biomedical Ethics Committee of the Health Science Center of Xi'an Jiaotong University (Approval No.: XJTUEA2023-1342).

Consent for Publication

All the authors agree to the publication of this work.

Author Contributions

All authors made a significant contribution to the work reported, including the conception, study design, execution, acquisition of data, analysis, and interpretation. They all participated in drafting, revising, or critically reviewing the article; provided final approval of the version to be published; and agreed to be accountable for all aspects of the work.

Funding

This work was supported by the Natural Science Foundation of Shaanxi Province (Grant no. 2022JM-546).

Disclosure

The authors declared no competing interests in this work.

References

1. Zhang J, Li S, Wu Y. Recovery of spinal cord injury following electroacupuncture in rats through enhancement of Wnt/β-catenin signaling. *Mol Med Rep*. 2017;16(2):2185–2190. doi:10.3892/mmr.2017.6801
2. Kang Y, Ding H, Zhou H, et al. Epidemiology of worldwide spinal cord injury: a literature review. *J Neurorestoratol*. 2018;6:1–9.
3. Tian T, Zhang S, Yang M. Recent progress and challenges in the treatment of spinal cord injury. *Protein Cell*. 2023;14(9):635–652. doi:10.1093/procel/pwad003
4. Ribeiro BF, Da Cruz BC, de Sousa BM, et al. Cell therapies for spinal cord injury: a review of the clinical trials and cell-type therapeutic potential. *Brain*. 2023;146(7):2672–2693. doi:10.1093/brain/awad047
5. Round JL, Mazmanian SK. The gut microbiota shapes intestinal immune responses during health and disease. *Nat Rev Immunol*. 2009;9(5):313–323. doi:10.1038/nri2515
6. Hooper LV, Littman DR, Macpherson AJ. Interactions Between the Microbiota and the Immune System. *Science*. 2012;336(6086):1268–1273. doi:10.1126/science.1223490
7. Nicholson JK, Holmes E, Kinross J, et al. Host-Gut Microbiota Metabolic Interactions. *Science*. 2012;336(6086):1262–1267. doi:10.1126/science.1223813
8. Willman J, Willman M, Reddy R, et al. Gut microbiome and neurosurgery: implications for treatment. *Clinical and Translational Discovery*. 2022;2(4). doi:10.1002/ctd2.139.
9. Agirman G, Hsiao EY. SnapShot: the microbiota-gut-brain axis. *Cell*. 2021;184(9):2524. doi:10.1016/j.cell.2021.03.022
10. Kirby T, Ochoa-Repáraz J. The Gut Microbiome in Multiple Sclerosis: a Potential Therapeutic Avenue. *Med Sci*. 2018;6(3):69. doi:10.3390/medsci6030069
11. Agirman G, Yu KB, Hsiao EY. Signaling inflammation across the gut-brain axis. *Science*. 2021;374(6571):1087–1092. doi:10.1126/science.abi6087
12. Calvani R, Picca A, Lo Monaco MR, Landi F, Bernabei R, Marzetti E. Of Microbes and Minds: a Narrative Review on the Second Brain Aging. *Front Med*. 2018;5(5):53. doi:10.3389/fmed.2018.00053
13. Rothhammer V, Mascanfroni ID, Bunse L, et al. Type I interferons and microbial metabolites of tryptophan modulate astrocyte activity and central nervous system inflammation via the aryl hydrocarbon receptor. *Nat Med*. 2016;22(6):586–597. doi:10.1038/nm.4106
14. Bazzocchi G, Turroni S, Bulzamini MC, et al. Changes in gut microbiota in the acute phase after spinal cord injury correlate with severity of the lesion. *Sci Rep-Uk*. 2021;11(1):12743.
15. Yuan B, Lu X, Wu Q. Gut Microbiota and Acute Central Nervous System Injury: a New Target for Therapeutic Intervention. *Front Immunol*. 2021;12:800796. doi:10.3389/fimmu.2021.800796
16. Chen S, Zhou Y, Chen Y, Gu J. fastp: an ultra-fast all-in-one FASTQ preprocessor. *Bioinformatics*. 2018;34(17):i884–i890. doi:10.1093/bioinformatics/bty560
17. Wood DE, Lu J, Langmead B. Improved metagenomic analysis with Kraken 2. *Genome Biol*. 2019;20(1):257. doi:10.1186/s13059-019-1891-0
18. Li D, Liu C, Luo R, Sadakane K, Lam T. MEGAHIT: an ultra-fast single-node solution for large and complex metagenomics assembly via succinct de Bruijn graph. *Bioinformatics*. 2015;31(10):1674–1676. doi:10.1093/bioinformatics/btv033
19. Steinegger M, Söding J. MMseqs2 enables sensitive protein sequence searching for the analysis of massive data sets. *Nat Biotechnol*. 2017;35(11):1026–1028. doi:10.1038/nbt.3988
20. Zhu W, Lomsadze A, Borodovsky M. Ab initio gene identification in metagenomic sequences. *Nucleic Acids Res*. 2010;38(12):e132. doi:10.1093/nar/gkq275
21. Cantalapiedra CP, Hernández-Plaza A, Letunic I, Bork P, Huerta-Cepas J. eggNOG-mapper v2: functional Annotation, Orthology Assignments, and Domain Prediction at the Metagenomic Scale. *Mol Biol Evol*. 2021;38(12):5825–5829. doi:10.1093/molbev/msab293
22. Bu D, Luo H, Huo P, et al. KOBAS-i: intelligent prioritization and exploratory visualization of biological functions for gene enrichment analysis. *Nucleic Acids Res*. 2021;49(W1):W317–W325. doi:10.1093/nar/gkab447
23. Segata N, Izard J, Waldron L, et al. Metagenomic biomarker discovery and explanation. *Genome Biol*. 2011;12(6):R60. doi:10.1186/gb-2011-12-6-r60
24. Ramette A. Multivariate analyses in microbial ecology. *Fems Microbiol Ecol*. 2007;62(2):142–160. doi:10.1111/j.1574-6941.2007.00375.x
25. Gunther J, Fallarino F, Fuchs D, Wirthgen E. Editorial: immunomodulatory Roles of Tryptophan Metabolites in Inflammation and Cancer. *Front Immunol*. 2020;11:1497. doi:10.3389/fimmu.2020.01497
26. Kigerl KA, Hall JC, Wang L, Mo X, Yu Z, Popovich PG. Gut dysbiosis impairs recovery after spinal cord injury. *J Exp Med*. 2016;213(12):2603–2620. doi:10.1084/jem.20151345
27. O'Connor G, Jeffrey E, Madorma D, et al. Investigation of Microbiota Alterations and Intestinal Inflammation Post-Spinal Cord Injury in Rat Model. *J Neurotraum*. 2018;35(18):2159–2166. doi:10.1089/neu.2017.5349

28. Zhang C, Zhang W, Zhang J, et al. Gut microbiota dysbiosis in male patients with chronic traumatic complete spinal cord injury. *J Transl Med*. 2018;16(1):353. doi:10.1186/s12967-018-1735-9
29. Zhang C, Jing Y, Zhang W, et al. Dysbiosis of gut microbiota is associated with serum lipid profiles in male patients with chronic traumatic cervical spinal cord injury. *Am J Transl Res*. 2019;11(8):4817–4834.
30. Yu B, Qiu H, Cheng S, et al. Profile of gut microbiota in patients with traumatic thoracic spinal cord injury and its clinical implications: a case-control study in a rehabilitation setting. *Bioengineered*. 2021;12(1):4489–4499. doi:10.1080/21655979.2021.1955543
31. Doelman A, Tigchelaar S, McConeghy B, et al. Characterization of the gut microbiome in a porcine model of thoracic spinal cord injury. *Bmc Genomics*. 2021;22(1):775. doi:10.1186/s12864-021-07979-3
32. Smith AM, Welch BA, Harris KK, Garrett MR, Grayson BE. Nutrient composition influences the gut microbiota in chronic thoracic spinal cord-injured rats. *Physiol Genomics*. 2022;54(10):402–415. doi:10.1152/physiolgenomics.00037.2022
33. Kong G, Zhang W, Zhang S, et al. The gut microbiota and metabolite profiles are altered in patients with spinal cord injury. *Mol Brain*. 2023;16(1):26. doi:10.1186/s13041-023-01014-0
34. Kang J, Sun Z, Li X, et al. Alterations in gut microbiota are related to metabolite profiles in spinal cord injury. *Neural Regen Res*. 2023;18(5):1076. doi:10.4103/1673-5374.355769
35. Cui Y, Liu J, Lei X, et al. Dual-directional regulation of spinal cord injury and the gut microbiota. *Neural Regen Res*. 2024;19(3):548–556. doi:10.4103/1673-5374.380881
36. Kaluzna-Czaplinska J, Gatarek P, Chirumbolo S, Chartrand MS, Bjorklund G. How important is tryptophan in human health? *Crit Rev Food Sci Nutr*. 2019;59(1):72–88. doi:10.1080/10408398.2017.1357534
37. Zelante T, Iannitti RG, Cunha C, et al. Tryptophan Catabolites from Microbiota Engage Aryl Hydrocarbon Receptor and Balance Mucosal Reactivity via Interleukin-22. *Immunity*. 2013;39(2):372–385. doi:10.1016/j.immuni.2013.08.003
38. Cervenka I, Agudelo LZ, Ruas JL. Kynurenines: tryptophan's metabolites in exercise, inflammation, and mental health. *Science*. 2017;357(6349):369.
39. Hou Y, Li J, Ying S. Tryptophan Metabolism and Gut Microbiota: a Novel Regulatory Axis Integrating the Microbiome, Immunity, and Cancer. *Metabolites*. 2023;13(11):1166. doi:10.3390/metabo13111166
40. Tian T, Mao Q, Xie J, et al. Multi-omics data reveals the disturbance of glycerophospholipid metabolism caused by disordered gut microbiota in depressed mice. *J Adv Res*. 2022;39:135–145. doi:10.1016/j.jare.2021.10.002
41. Dodd D, Spitzer MH, Van Treuren W, et al. A gut bacterial pathway metabolizes aromatic amino acids into nine circulating metabolites. *Nature*. 2017;551(7682):648–652. doi:10.1038/nature24661
42. Wang G, Fan Y, Zhang G, et al. Microbiota-derived indoles alleviate intestinal inflammation and modulate microbiome by microbial cross-feeding. *Microbiome*. 2024;12(1):59. doi:10.1186/s40168-024-01750-y
43. Sinha AK, Laursen MF, Brinck JE, et al. Dietary fibre directs microbial tryptophan metabolism via metabolic interactions in the gut microbiota. *Nat Microbiol*. 2024;9(8):1964–1978. doi:10.1038/s41564-024-01737-3
44. Montgomery TL, Eckstrom K, Lile KH, et al. Lactobacillus reuteri tryptophan metabolism promotes host susceptibility to CNS autoimmunity. *Microbiome*. 2022;10(1):198. doi:10.1186/s40168-022-01408-7
45. Xiao L, Yan J, Yang T, et al. Fecal Microbiome Transplantation from Children with Autism Spectrum Disorder Modulates Tryptophan and Serotonergic Synapse Metabolism and Induces Altered Behaviors in Germ-Free Mice. *Msystems*. 2021;6(2):e1320–e1343. doi:10.1128/msystems.01343-20
46. Liu Z, Ling Y, Peng Y, et al. Regulation of serotonin production by specific microbes from piglet gut. *J Anim Sci Biotechnol*. 2023;14(1):111. doi:10.1186/s40104-023-00903-7
47. Chen CM, Wu CC, Huang CL, et al. Lactobacillus plantarum PS128 Promotes Intestinal Motility, Mucin Production, and Serotonin Signaling in Mice. *Probiotics Antimicrob Proteins*. 2022;14(3):535–545. doi:10.1007/s12602-021-09814-3
48. Cervantes-Barragan L, Chai JN, Tianero MD, et al. Lactobacillus reuteri induces gut intraepithelial CD4(+)CD8alphaalpha(+) T cells. *Science*. 2017;357(6353):806–810. doi:10.1126/science.aah5825
49. Pan T, Pei Z, Fang Z, et al. Uncovering the specificity and predictability of tryptophan metabolism in lactic acid bacteria with genomics and metabolomics. *Front Cell Infect Microbiol*. 2023;13:1154346. doi:10.3389/fcimb.2023.1154346
50. Marcial GE, Ford AL, Haller MJ, et al. Lactobacillus johnsonii N6.2 Modulates the Host Immune Responses: a Double-Blind, Randomized Trial in Healthy Adults. *Front Immunol*. 2017;8:655. doi:10.3389/fimmu.2017.00655
51. Jia L, Xiao L, Fu Y, et al. Neuroprotective effects of probiotics on anxiety- and depression-like disorders in stressed mice by modulating tryptophan metabolism and the gut microbiota. *Food Funct*. 2024;15(6):2895–2905. doi:10.1039/D3FO03897A
52. Rothhammer V, Borucki DM, Tjon EC, et al. Microglial control of astrocytes in response to microbial metabolites. *Nature*. 2018;557(7707):724–728. doi:10.1038/s41586-018-0119-x
53. Chen Y, Wang Y, Fu Y, Yin Y, Xu K. Modulating AHR function offers exciting therapeutic potential in gut immunity and inflammation. *Cell Biosci*. 2023;13(1):85. doi:10.1186/s13578-023-01046-y
54. Lamas B, Richard ML, Leducq V, et al. CARD9 impacts colitis by altering gut microbiota metabolism of tryptophan into aryl hydrocarbon receptor ligands. *Nat Med*. 2016;22(6):598–605. doi:10.1038/nm.4102
55. Kameda K, Someya S, Fujita J, Fukuda K, Tohyama S. Protocol for enhanced proliferation of human pluripotent stem cells in tryptophan-fortified media. *STAR Protoc*. 2022;3(2):101341. doi:10.1016/j.xpro.2022.101341
56. Xu K, Fu Y, Gao H, Bai M, Liu H, Duan Y. L-Tryptophan activates the aryl hydrocarbon receptor and induces cell cycle arrest in porcine trophectoderm cells. *Theriogenology*. 2021;171:137–146. doi:10.1016/j.theriogenology.2021.05.012
57. Wang H, Ji Y, Wu G, et al. l-Tryptophan Activates Mammalian Target of Rapamycin and Enhances Expression of Tight Junction Proteins in Intestinal Porcine Epithelial Cells. *J Nutr*. 2015;145(6):1156–1162. doi:10.3945/jn.114.209817
58. Xu F, Na L, Li Y, Chen L. Roles of the PI3K/AKT/mTOR signalling pathways in neurodegenerative diseases and tumours. *Cell Biosci*. 2020;10(1):54. doi:10.1186/s13578-020-00416-0
59. Cheng P, Liao HY, Zhang HH. The role of Wnt/mTOR signaling in spinal cord injury. *J Clin Orthop Trauma*. 2022;25:101760. doi:10.1016/j.jcot.2022.101760